

Effect of Sintering Temperature and Applied Pressure on the Properties of Boron Carbide-Silicon Carbide Composites

Zeynep Aygüzer Yaşar^a and Richard A. Haber^{b, *}

^a Department of Metallurgical and Materials Engineering, Hitit University, Corum, 19030 Turkey

^b Department of Material Science and Engineering, Rutgers, The State University of New Jersey, Piscataway, NJ, 08854 USA

*e-mail: rich.haber@rutgers.edu

Received January 15, 2021; revised March 1, 2021; accepted March 9, 2021

Abstract—To obtain high density boron carbide-silicon carbide composites, the spark plasma sintering method was used. 50% B₄C–1.5% C–48.5% SiC mixture compositions were sintered at four different temperatures (1800, 1850, 1900, 1950°C) under 50 MPa pressure and four different applied pressures (20, 30, 40, and 50 MPa) at a constant temperature of 1950°C. The boron carbide-silicon carbide composites reached full density (>99% th. density) at 1950°C and under 50 MPa pressure. Samples were characterized using SEM, XRD, and ultrasound analysis. Density, Vickers hardness, Berkovich hardness and fracture toughness were also evaluated. Ultrasound analysis showed that increasing the sintering temperature and applied pressure increased the elastic modulus, shear, and bulk modulus of the composites. The samples densified at 1950°C under 50 MPa pressure, had 409 GPa elastic modulus, 176 GPa shear modulus, and 203 GPa bulk modulus. With increasing sintering temperature and pressure, the hardness and fracture toughness of the composites also increased. Vickers hardness values dramatically increased from 17.55 GPa (1800°C) to 30.78 GPa (1950°C) with increasing sintering temperature. The highest Berkovich hardness value was obtained as 37.37 GPa in the sample sintered at 1950°C under 50 MPa. The highest calculated fracture toughness values were 2.64 MPa m^{1/2} (1950°C under 50 MPa).

Keywords: silicon carbide, boron carbide, spark plasma sintering, mechanical properties, microstructure

DOI: 10.3103/S1063457621060022

1. INTRODUCTION

Both boron carbide and silicon carbide have superior physical and chemical properties [1, 2]. For instance, boron carbide is a low-density material of 2.52 g/cm³ [3, 4], with superior hardness and elastic modulus. Boron carbide also has a high melting point, strength, neutron cross-section, wear resistance, and elevated chemical stability [5–12]. SiC has a relatively low theoretical density of 3.21 g/cm³, a high hardness and elastic modulus, high oxidation resistance, superior wear resistance, good thermal conductivity, and thermal shock resistance [5, 13–19]. Due to their outstanding properties, boron carbide-silicon carbide composites are used as nozzles, in turbine engines, heat conducting tubes, and in the defense industry (armor plate) [20, 21]. However, it is difficult to obtain sintered composite bodies with high density without applying pressure or sintering aids because of the strong covalent bonding [22–25]. Studies have shown that SiC has improved the sinterability of B₄C without worsening the properties. For this reason, B₄C-SiC composites have gained importance [26]. For example, a commercially available pressure-assisted densification (PAD)-B₄C (hot pressed) has 25.82 GPa hardness while a B₄C-SiC composite containing only 50% B₄C has a hardness of 30.34 GPa [11, 27]. In addition to improve the sinterability of boron carbide-silicon carbide composites Al, Si, TiC, ZrB₂, TiB₂, Al₂O₃, Y₂O₃, TiH₂ and graphite have been used as sintering aids [28, 29].

There are number of ways to sinter boron carbide-silicon carbide composites including pressureless sintering, hot pressing and spark plasma sintering with solid state or liquid phase sintering [9, 30–32].

In this research the spark plasma sintering (SPS) method was used to achieve higher densities in shorter times without grain growth at relatively low temperature [13, 33, 34].

The aim of this study was to investigate the effect of sintering temperature and applied pressure on the elastic and mechanical properties of boron carbide-silicon carbide composites and to produce high density ceramic composites with uniform distribution and small particle size. To achieve this goal, boron carbide-silicon carbide composites were densified at four different sintering temperatures and four different applied pressures. The spark plasma sintering method was used to densify these boron carbide-silicon carbide composites with carbon additives.

2. EXPERIMENTAL

Commercial raw materials were used for this research: silicon carbide (UF-25, H.C. Starck GmbH&Co., Germany), boron carbide (HD-20, H.C. Starck GmbH&Co., Germany), and carbon (Lamp black from Fisher Scientific). The average particle sizes of both silicon carbide and boron carbide were 0.6 μm . To produce all samples, 50 wt % B_4C –1.5 wt % C–48.5 wt % SiC powders were mixed by ball milling in an ethanol for 24 h with silicon carbide balls. It was not aimed to reduce the particle size of the powders. Ball mill was a low energy mill used to mix powders evenly. The liquid mixture was dried using a hot plate at 275°C. Then the dry powder chunks were ground with mortar and pestle. Samples were sintered using the spark plasma sintering method (Thermal Technology SPS 10-4) with 5 grams of each powder mixture in a 20 mm inner diameter graphite die lined with graphite foil. The graphite die had a small hole drilled partially through the wall mid-way along its length. An optical pyrometer pointed at this hole to measure the temperature of the sample during the heating cycle.

To find the optimal sintering temperature boron carbide-silicon carbide composites were sintered at four different temperatures of 1800, 1850, 1900, and 1950°C. Samples were heated to an intermediate dwell of 1400°C with a 200°C/min heating rate under a vacuum and 50 MPa applied pressure. After 1 min at 1400°C, the samples were heated to the sintering temperature at 200°C/min under 50 MPa applied pressure and held for 5 min.

To find the optimal applied pressure boron carbide-silicon carbide composites were sintered at 1950°C with four different applied pressures of 20, 30, 40, and 50 MPa. Samples were heated to 1400°C with a 200°C/min heating rate under vacuum and 20, 30, 40, or 50 MPa applied pressure. After 1 minute at 1400°C, the samples were heated to 1950°C at 200°C/min, maintaining at the same applied pressure and held for 5 min.

After sintering, each sample required sandblasting upon removal from the SPS die to remove a layer of graphite foil that remained from the sintering process. Surface grinding was necessary after sand blasting to produce a smooth and flat surface for ultrasound analysis and X-ray diffraction since the samples had remaining carbon from the graphite foil and imperfections from sandblasting. The density was measured after surface grinding using Archimedes' method. Then, the samples were cut using a LECO Vari/Cut 50 diamond saw and mounted in epoxy using a Buehler SimpliMet 1000 mounting press. Samples were then polished to a 0.25 μm finish using Buehler-Ecomet 250-Grinder-Polisher. Another small piece was cut, and cross section milled for 5 h with 6 kV acceleration voltage using a Hitachi IM4000 Plus ion milling system. After cross sectioning, samples were flat milled for 5 min at 80° tilt angle with 3 kV acceleration voltage to remove imperfections from the sample surfaces.

Microstructural analysis was carried out on sintered dense composite samples. The Zeiss Sigma field emission scanning electron microscope was used to define pores, inhomogeneities, grain size, and shape. The linear intercepts method was used to measure grain size using Lince 2.4.2 image analysis software, and at least a hundred grains were measured. XRD diffraction analysis was done using a Panalytical X'Pert X-Ray diffractometer to determine the phase composition.

Elastic properties of dense composite samples were measured by ultrasound analysis according to ASTM standard E494-10 [35] using single transducers in a pulsed-echo configuration where the same transducer both emits and receives ultrasonic energy. Using an Olympus V316 transducer (Olympus Corporation, Tokyo, Japan) longitudinal time of flight (LTOF) was measured with the sample immersed in water. Shear time of flight (STOF) was measured (using Sonotech Shear Gel as a couplant) using an Olympus V222-BA-RM shear contact transducer. Using measured LTOF and STOF values, the longitudinal (c_L) and shear (c_S) sound speeds values were calculated according to the following equations:

$$c_L = \frac{2d}{\text{LTOF}}, \quad (1)$$

$$c_S = \frac{2d}{\text{STOF}}, \quad (2)$$

where d is the thickness of the sample. Poisson's ratio (ν), Young's modulus (E), bulk modulus (K), and shear modulus (G) were calculated by the following equations:

Poisson's ratio:

$$\nu = \frac{1 - 2\left(\frac{c_S}{c_L}\right)^2}{2 - 2\left(\frac{c_S}{c_L}\right)^2}. \quad (3)$$

Young's modulus:

$$E = \frac{(1 - 2\nu)(1 + \nu)\rho c_L^2}{1 - \nu}. \quad (4)$$

Bulk modulus:

$$K = \frac{E}{3(1 - 2\nu)}. \quad (5)$$

Shear modulus:

$$G = \frac{E}{2(1 + \nu)}. \quad (6)$$

Vickers hardness was measured using a LECO M-400-G3 microhardness tester. Ten acceptable indentations were made for 9.8 N load with an holding time of 10 s. Indent sizes were measured using a Keyence VHX 5000 digital microscope.

By the following equation, Vickers hardness value was calculated referring to ASTM C1327-15 [36]:

$$H_v \text{ (GPa)} = 1.8544 \frac{P}{d^2}, \quad (7)$$

where P (kgf) is the applied load, and d (mm) is the average length of the two diagonals of the indentation. The reported hardness value presents the mean of the calculated hardness values from the 10 indents.

The indentation fracture toughness was calculated by measuring Vickers indentation crack lengths. Each reported indentation fracture toughness value presents the mean of the calculated fracture toughness from 10 indents. Indentation fracture toughness was calculated by the following equation [37]:

$$K_c = 0.018(E/H_v)^{0.5} (P/c^{1.5}). \quad (8)$$

Using the Micromaterials NanoTest Vantage tester with Berkovich indenter, nanoindentation test also was performed on the B_4C -SiC composites. For this test, 20 indents were made for 200 mN load on the polished sample surfaces. Then the hardness values of samples were calculate using the MicroMateriaks software.

3. RESULTS AND DISCUSSION

3.1. Effect of Sintering Temperature

The density values of the spark plasma sintered samples were measured using the Archimedes' method and theoretical density of the samples were determined by the rule of mixtures. Table 1 shows the sintering conditions and relative density of the samples. It can be seen that the sample sintered at 1950°C with 50 MPa applied pressure was almost fully dense. Also, it may be seen that there was a significant increment in relative density from 93.59 to 99.64% moving from the sample sintered at 1800°C to that sintered at 1950°C. As can be seen from the density values, highly dense B_4C -SiC composites can be obtained with a short sintering time at relatively low temperature with the SPS method. Zhang et al. densified B_4C -SiC samples at 2300°C for 16 h by pressureless sintering method and only could be reached 93.9% theoretical density [38].

The influence of sintering temperature on the relative density can be seen in Fig. 1. Each density value represents the mean of five measurements. It can be concluded that the density of the material increases as the sintering temperature increases. Increasing the sintering temperature, increases the diffusion between particles, in turn increasing the density of the materials. Zhang et al. sintered B_4C -SiC compos-

Table 1. SPS sintering conditions for the effect of sintering temperature

Sample	Sintering temperature, °C	Applied pressure, MPa	Dwelling time, min	Density, g/cm ³	Theoretical density, g/cm ³	Average percent density, %
1400-1-1800-5-50	1800	50	5	2.630 ± 0.002	2.81	93.59
1400-1-1850-5-50	1850	50	5	2.730 ± 0.002	2.81	97.15
1400-1-1900-5-50	1900	50	5	2.770 ± 0.001	2.81	98.57
1400-1-1950-5-50	1950	50	5	2.800 ± 0.002	2.81	99.64

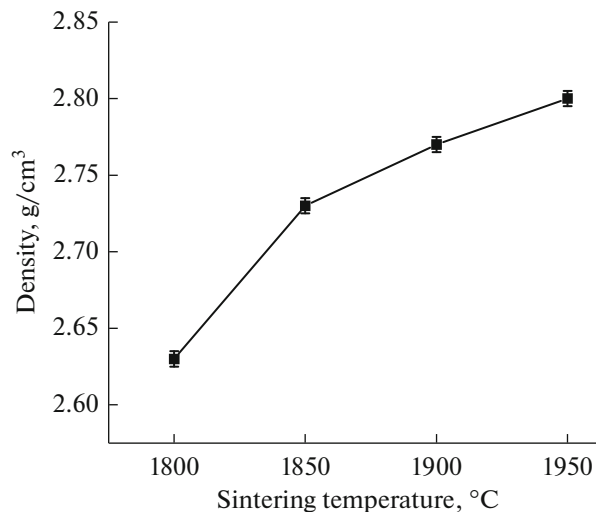
ites at 1800, 1900 and 1950°C under 30 MPa applied pressure for 60 min with hot press and their relative densities were 68.0, 97.2 and 98.6%, respectively [39]. When comparing the results in the literature [39] with the results in this study, it is possible to conclude that SPS helps to achieve higher density than hot press.

In Fig. 2, the microstructure images for the samples sintered at different temperatures can be seen. The light areas are silicon carbide (SiC), and the dark areas are boron carbide (B₄C). The images confirmed the Archimedes' density results since they showed irregular pores at the low sintering temperature and a fully dense microstructure at 1950°C. When looking at the study of Zhang et al. [39] with the hot press method, the samples were not dense at 1800°C and extremely large pores were observed. Likewise, the pores can be easily seen in the sample sintered at 1900°C. However, looking at the SEM images in this study, it can be clearly seen that this problem does not exist as all of the samples densified with only small pores.

The average grains size of boron carbide and silicon carbide with standard deviations can be seen in Table 2. Even with increasing sintering temperature, the boron carbide and silicon carbide grains remained below 0.5 µm. SPS sintering did not cause significant grain growth compared to the initial size of the powders. In the literature, the average grain size of B₄C–SiC composite samples densified by hot press was found to be 2 µm [39].

In Fig. 3 X-ray diffraction patterns of the samples sintered at different temperatures are displayed. All samples showed similar XRD patterns with silicon carbide, boron carbide and a small amount of carbon as expected. Compared with raw starting materials, no byproducts were formed. Since the composites were not made from in-situ processing, the sintering temperature did not affect the peak intensity and therefore the relative amount of the main phases.

The samples' elastic properties were measured using ultrasound analysis. Each value represents the mean of five measurements. Longitudinal sound speed (c_L), shear sound speed (c_S), Poisson's ratio, Young's modulus (E), shear modulus (G), and bulk modulus (K) values can be seen in Table 3. The elastic properties have a direct relation to density, and therefore they all increased with increasing sintering tem-

**Fig. 1.** Effect of the sintering temperature on the density.

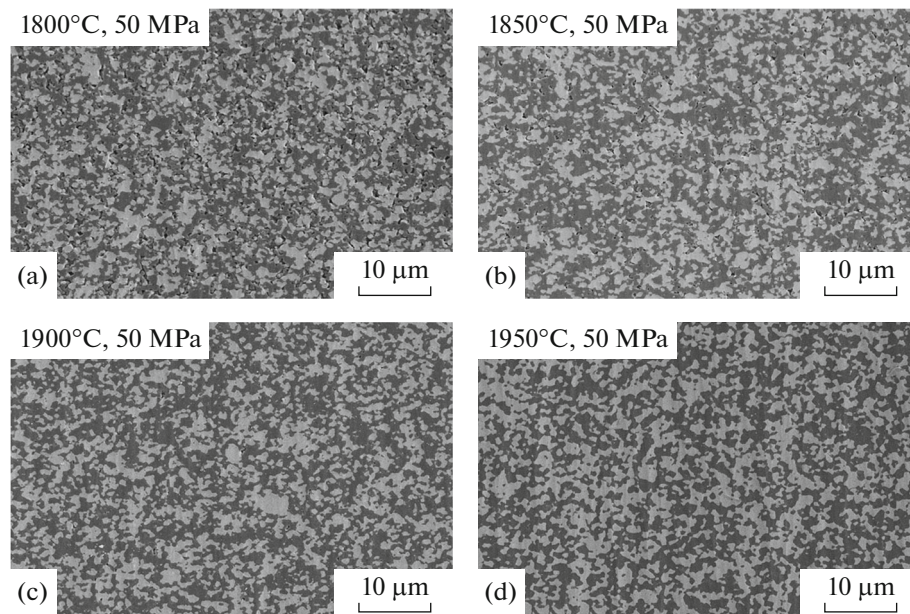


Fig. 2. Microstructure images of 50% B₄C–1.5% C–48.5% SiC samples sintered at 1800, 1850, 1900, and 1950°C.

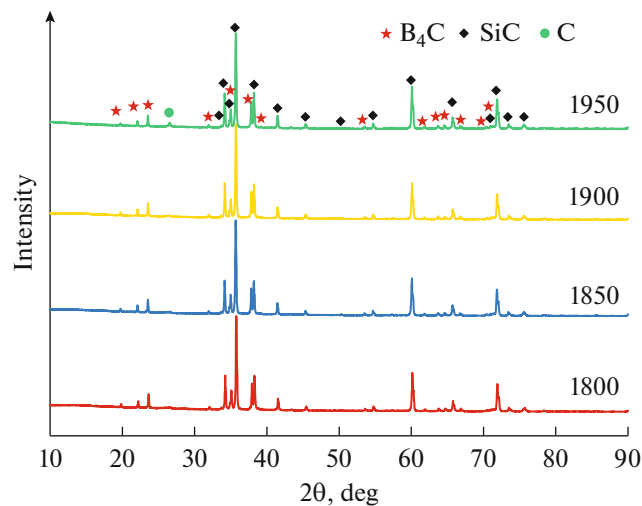


Fig. 3. X-ray diffraction patterns of 50% B₄C–1.5% C–48.5% SiC samples sintered at 1800, 1850, 1900, and 1950°C.

perature. When the sintering temperature increased from 1800 to 1950°C, the Poisson's ratio value increased from 0.160 to 0.165, Young's modulus showed a significant increase from 333 to 409 GPa, the shear modulus changed from 144 to 176 GPa, and the bulk modulus increased from 163 to 203 GPa. Thu-

Table 2. Average grain sizes for different sintering temperatures

Sample	Average grain size of B ₄ C, µm (Std. Dev)	Average grain size of SiC, µm (Std. Dev)
1400-1-1800-5-50	0.46 ± 0.05	0.31 ± 0.03
1400-1-1850-5-50	0.44 ± 0.04	0.34 ± 0.03
1400-1-1900-5-50	0.43 ± 0.04	0.41 ± 0.04
1400-1-1950-5-50	0.44 ± 0.04	0.44 ± 0.04

Table 3. Elastic properties of 50% B₄C–1.5% C–48.5% SiC samples sintered at 1800, 1850, 1900, and 1950°C

Sample	c_L , m/s	c_S , m/s	Poisson's ratio	E , GPa	G , GPa	K , GPa
1400-1-1800-5-50	11611	7387	0.160 ± 0.003	333 ± 7	144 ± 3	163 ± 3
1400-1-1850-5-50	12525	7944	0.163 ± 0.003	401 ± 8	172 ± 3	199 ± 4
1400-1-1900-5-50	12523	7928	0.166 ± 0.003	405 ± 8	174 ± 4	202 ± 4
1400-1-1950-5-50	12506	7921	0.165 ± 0.003	409 ± 8	176 ± 4	203 ± 4

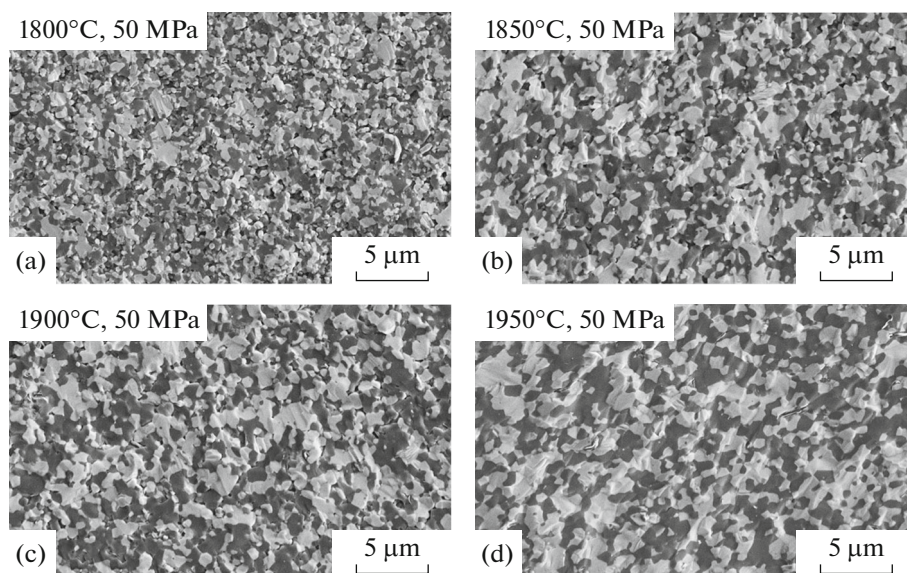
ault et al. processed B₄C–SiC composites via reaction bonding method, and the samples containing 85% B₄C obtained by this method could only reach an elastic modulus value of 309 GPa [40]. Similar results were also found in literature as Hayun et al. measured the elastic modulus of the B₄C–SiC composite as 360 GPa [41]. Although this value is higher than Thuault's value, it is still considerably lower than the value of elastic modulus obtained in this study.

To determine the fracture mode of the composites, SEM imaging was used. Figure 4 shows the fracture surfaces of samples sintered at different temperatures. From the images it can be seen that the composites have a transgranular fracture mode.

Figure 5 shows indentation cracks in polished surfaces. The images show that the composites mostly have a transgranular fracture mode and the crack propagated straight without any deflection due to the similar thermal expansion coefficient. The different sintering temperatures did not affect the fracture mode of the composites.

In Table 4, hardness and fracture toughness results are shown. Each value represents the mean of ten calculated hardness and indentation fracture toughness values. The measured Vickers hardness results showed that with increasing sintering temperature, the composite's hardness is enhanced. Since the porosity diminished with increasing sintering temperature, it showed a positive beneficial outcome on the materials hardness. In the study of Zhu et al. it is clear how density affects the hardness as the composite material with 85% B₄C content could only reach a hardness value of 20 GPa because its density was only 85% [26]. It would have been expected to have a higher hardness value due to its high B₄C content, but the low density prevented this. Since a high density value was reached in this study, the composite containing 50% B₄C was able to reach a very high hardness value.

Similar to Vickers hardness, Berkovich hardness values increased from 21.19 to 37.37 GPa when the sintering temperature increased. Since the Berkovich (nanoindentation) test is performed with smaller loads, it shows higher results compared to the Vickers test. Dub et.al. performed nanoindentation to B₄C

**Fig. 4.** Fracture surface images of 50% B₄C–1.5% C–48.5% SiC samples sintered at 1800, 1850, 1900, and 1950°C.

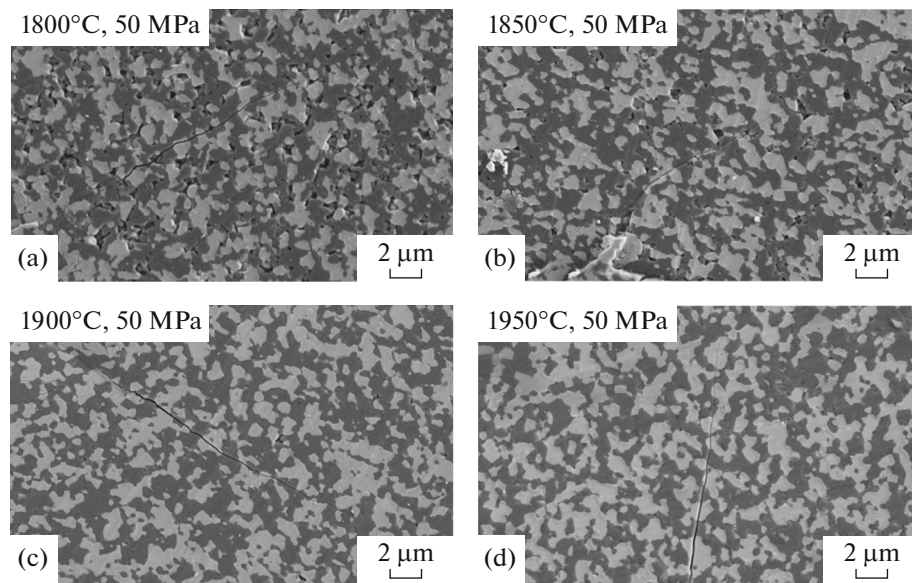


Fig. 5. Indentation crack in polished surfaces images of 50% B_4C –1.5% C–48.5% SiC samples sintered at 1800, 1850, 1900, and 1950°C.

at 10mN and obtained a hardness value of 45.3 GPa [42]. When this hardness value is compared with the hardness value of current research, although it contains only 50% B_4C , a quite high hardness value was obtained at a loading value of 200 mN.

Since the sample that was sintered at 1800°C had pores on the surface, the crack length and fracture toughness could not be measured. Fracture toughness values were very similar despite the different densities of the samples.

3.2. Effect of Applied Pressure

Table 5 shows the sintering conditions and relative densities of the samples obtained at 1950°C with different applied pressures. It is observed that the sample sintered at 1950°C with 50 MPa applied pressure is almost fully dense. The relative density changed from 98.57 to 99.64% with increasing pressure. Zhu et al. densified B_4C –SiC composites with pressureless sintering method at 2150°C for 60 min and the sample could only reach 85% of its theoretical density [26]. With the SPS method, a density value higher than this value was obtained even at a relatively low pressure such as 20 MPa.

In the present study, samples sintered with SPS for 5 min below 30 MPa at 1950°C reached 98.93% relative density. In literature, samples sintered by hot pressing at 1950°C under 30 MPa pressure for 30 min could only reach 96% relative density [43]. Even at the same temperature and pressure and shorter dwelling time, the SPS method has provided higher density than the hot press method.

The effect of applied pressure on the density can be seen in Fig. 6. It may be seen that the relative density of the materials increased with increasing applied pressure. Increasing the applied pressure increased the diffusion between particles so that the material's density also increased.

Table 4. Effect of sintering temperature on hardness and indentation fracture toughness

Sample	Vickers hardness, GPa	Fracture toughness, MPa m ^{1/2}	Berkovich hardness, GPa
1400-1-1800-5-50	17.55 ± 0.78	–	21.19 ± 1.90
1400-1-1850-5-50	28.63 ± 1.11	2.50 ± 0.05	35.43 ± 1.27
1400-1-1900-5-50	28.91 ± 0.68	2.60 ± 0.14	36.70 ± 1.47
1400-1-1950-5-50	30.78 ± 1.79	2.64 ± 0.24	37.27 ± 1.88

Table 5. SPS conditions for the effect of applied pressure

Sample	Sintering temperature, °C	Applied pressure, MPa	Dwelling time, min	Density, g/cm ³	Theoretical density, g/cm ³	Average percent density, %
1400-1-1950-5-20	1950	20	5	2.770 ± 0.004	2.81	98.57
1400-1-1950-5-30	1950	30	5	2.780 ± 0.002	2.81	98.93
1400-1-1950-5-40	1950	40	5	2.790 ± 0.006	2.81	99.28
1400-1-1950-5-50	1950	50	5	2.800 ± 0.002	2.81	99.64

Table 6. Average grain sizes for different applied pressures

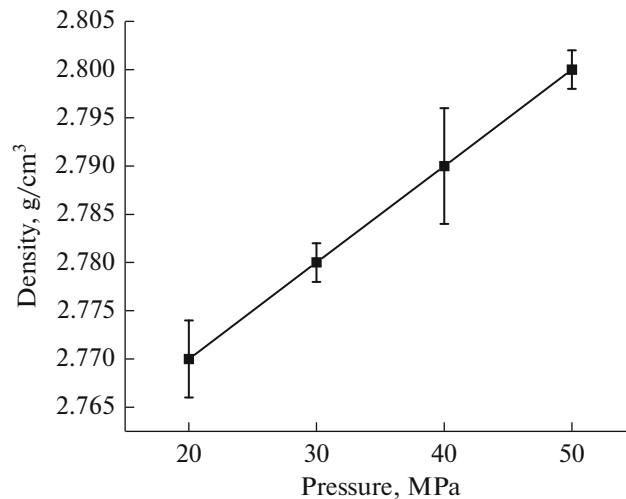
Sample	Average grain size of B ₄ C, μm (std. dev)	Average grain size of SiC, μm (std. dev)
1400-1-1950-5-20	0.63 ± 0.05	0.53 ± 0.05
1400-1-1950-5-30	0.51 ± 0.04	0.51 ± 0.05
1400-1-1950-5-40	0.50 ± 0.07	0.43 ± 0.07
1400-1-1950-5-50	0.44 ± 0.04	0.44 ± 0.04

Figure 7 displays the microstructure images for samples sintered under different applied pressures. The light areas are SiC, and the dark areas are B₄C. The microstructure images support the Archimedes density results. Even at the lower applied pressure (20 MPa), pores could not be seen.

The average grain sizes of boron carbide and silicon carbide grains with standard deviations for different applied pressures are shown in Table 6. Increasing the applied pressure from 20 to 50 MPa at the same sintering temperature, did not cause the boron carbide or silicon carbide grains to coarsen.

In Fig. 8, X-ray diffraction patterns of the samples sintered at different pressures can be seen. All samples contained the nominal phases: silicon carbide, boron carbide were observed as the major phases and carbon was the minor phase.

The samples longitudinal sound speed (c_L), shear sound speed (c_S), Poisson's ratio, Young's modulus (E), shear modulus (G), and bulk modulus (K) values are summarized in Table 7. Due to the strong relation between relative densities and elastic properties, the elastic modulus, bulk modulus, and shear modulus increased with increasing sintering applied pressure. The Poisson's ratio changed from 0.160 to 0.165, the Young's modulus increased from 390 to 409 GPa, the shear modulus increased from 168 to 176 GPa, and the bulk modulus increased from 192 to 203 GPa.

**Fig. 6.** Effect of the applied pressure on the density.

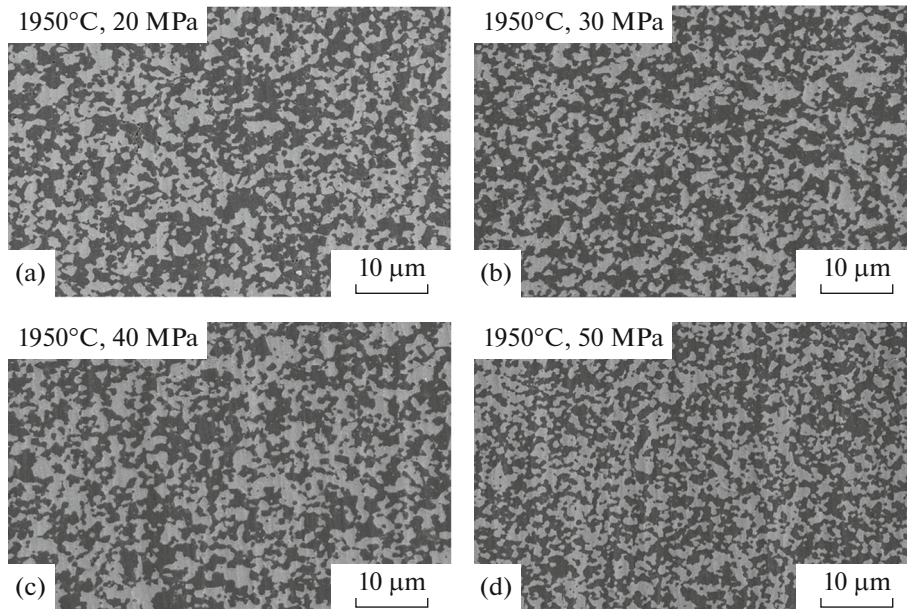


Fig. 7. Microstructure images of 50% B_4C –1.5% C–48.5% SiC samples sintered at 1950°C under different applied pressures 20, 30, 40, and 50 MPa.

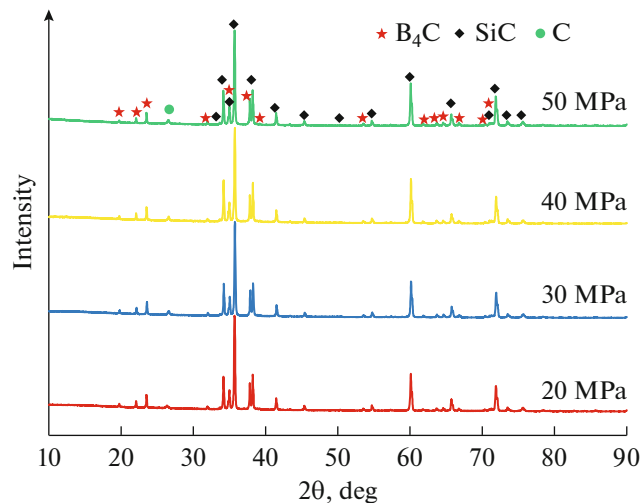


Fig. 8. X-ray diffraction patterns of 50% B_4C –1.5% C–48.5% SiC samples sintered at 1950°C under different applied pressures 20, 30, 40, and 50 MPa.

Figure 9 shows the fracture surfaces of samples sintered at 1950°C with different applied pressures. Microstructure images showed that composites showed transgranular fracture mode.

Figure 10 shows indentation cracks in the polished surfaces. From the images show that the composites have a transgranular fracture mode. Changing the applied pressure from 20 to 50 MPa did not affect the fracture mode of the composites, with the cracks propagating straight in each case.

In Table 8, the hardness and fracture toughness results are shown. The Vickers hardness values show that by increasing the applied pressure at the same sintering temperature, the composite's Vickers hardness also increased. It is again related to the amount of porosity in the samples; if porosity decreases with increasing pressure, then the hardness increases. Zhang et al. [43] sintered their samples with a hot press at 1950°C under 30 MPa pressure and the hardness value of the samples was only 24 GPa. In this study, the hardness of the samples sintered with SPS at the same temperature and pressure reached 28.76 GPa. Using only a different sintering method, the hardness of the sample with the same composition increased

Table 7. Elastic properties of 50% B₄C–1.5% C–48.5% SiC samples sintered at 1950°C under different applied pressures 20, 30, 40, and 50 MPa

Sample	c_L , m/s	c_S , m/s	Poisson's ratio	E , GPa	G , GPa	K , GPa
1400-1-1950-5-20	12254	7794	0.160 ± 0.003	390 ± 8	168 ± 3	192 ± 4
1400-1-1950-5-30	12398	7852	0.165 ± 0.003	400 ± 8	172 ± 3	199 ± 4
1400-1-1950-5-40	12457	7891	0.165 ± 0.003	406 ± 8	174 ± 4	202 ± 4
1400-1-1950-5-50	12506	7921	0.165 ± 0.003	409 ± 8	176 ± 4	203 ± 4

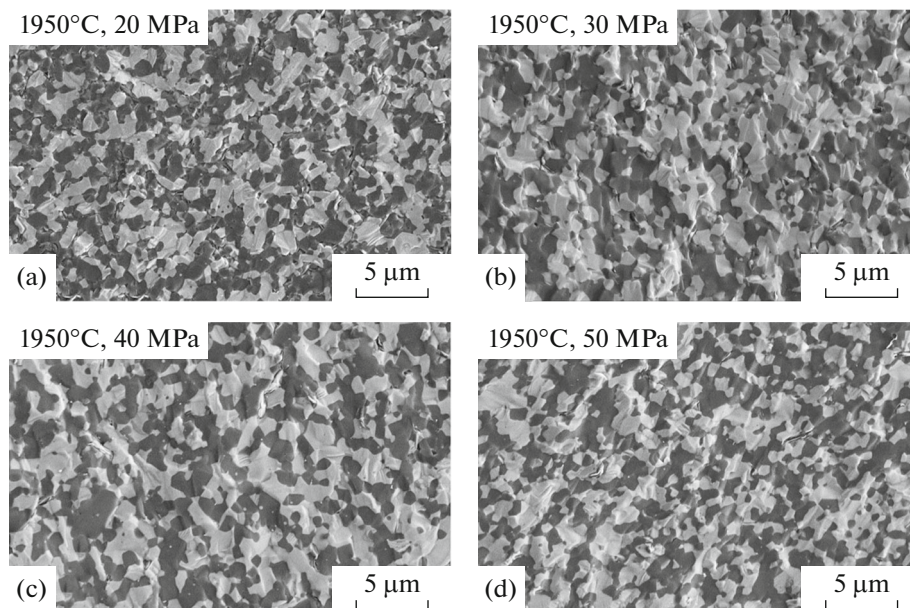
Table 8. Effect of applied pressure on hardness and indentation fracture toughness

Sample	Hardness, GPa	Fracture toughness, MPa m ^{1/2}	Berkovich hardness, GPa
1400-1-1950-5-20	28.72 ± 0.72	2.65 ± 0.06	27.10 ± 1.67
1400-1-1950-5-30	28.76 ± 1.01	2.69 ± 0.07	34.87 ± 1.49
1400-1-1950-5-40	29.21 ± 0.48	2.72 ± 0.19	35.12 ± 1.49
1400-1-1950-5-50	30.78 ± 1.79	2.64 ± 0.24	37.27 ± 1.88

by approximately 20%. Adding different additives to B₄C may also cause changes in the hardness values of the samples. For example Ivzhenko et.al. added different proportions of TiH₂ to B₄C. Active Ti was obtained by the decomposition of TiH₂. However, the hardness values decreased when the amount of Ti increase in the composite. The highest hardness value was obtained at 23.3 GPa and 2.8 vol. % Ti content [29].

Similar to Vickers hardness, Berkovich hardness values increased from 27.10 to 37.37 GPa when the applied pressure increased at the same sintering temperature.

Fracture toughness values did not vary much with applied pressure and density and were all in a narrow range from 2.63–2.71 MPa m^{1/2}. Since the B₄C and SiC have similar thermal expansion of coefficient, addition of SiC to B₄C did not cause deflection in cracks. However, Ivzhenko et al. showed that fracture toughness increased due to TiB₂ formation as a result of the reaction of Ti in the composite with C. Since

**Fig. 9.** Fracture surfaces of 50% B₄C–1.5% C–48.5% SiC samples sintered at 1950°C under different applied pressures 20, 30, 40, and 50 Mpa.

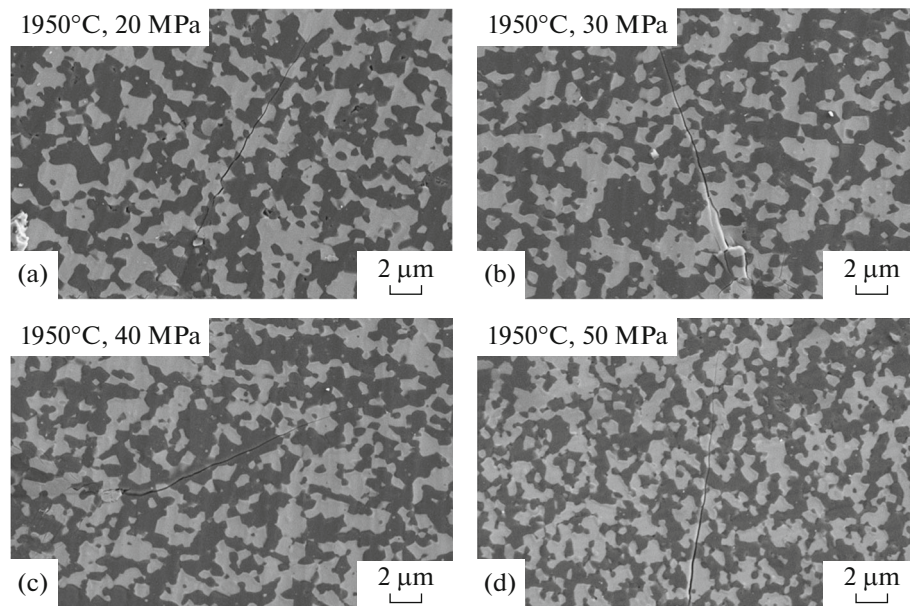


Fig. 10. Intentional cracks in polished surfaces images of 50% B_4C –1.5% C–48.5% SiC samples sintered at 1950°C under different applied pressures 20, 30, 40, and 50 MPa.

the thermal expansion coefficients of TiB_2 and B_4C are very different, TiB_2 in the composites caused deflection in the cracks.

4. CONCLUSIONS

In this research, SiC– B_4C composites were produced by spark plasma sintering at different peak temperature or applied pressures. The sintering temperatures, held for 5 min, were 1800, 1850, 1900, 1950°C with 50 MPa applied pressure. The applied pressures varied from 20, 30, 40 and 50 MPa with a fixed temperature of 1950°C for 5 min.

The sinterability of the composite was increased by increasing the sintering temperature and the pressure which enhanced the diffusion mechanism and the bonding between particles. Ultrasound analysis confirmed a direct relationship between density and elastic modulus, shear, bulk modulus and hardness. The samples sintered at 1950°C had 409 GPa elastic modulus, 176 GPa shear modulus, 203 GPa bulk modulus, 31 GPa Vickers hardness, and 37.27 GPa Berkovich hardness. Fracture toughness was unaffected by any of the changed parameters.

The results confirmed that to densify SiC– B_4C composites high temperatures and high pressures are required. However, it seems that sintering temperature has a greater influence on the final density as compared to the applied pressure. Indeed, the sample sintered at the lowest temperature, 1800°C with 50 MPa, had lower density as compared to the sample sintered at the lowest pressure, 1950°C with 20 MPa, 93.6 and 98.6% respectively.

FUNDING

Research was sponsored by the National Science Foundation I/UCRC Award no. 1540027. The views and conclusions contained in this document are those of the authors and should not be interpreted as representing the official policies, either expressed or implied, of the National Science Foundation or the U.S. Government. The U.S. Government is authorized to reproduce and distribute reprints for Government purposes notwithstanding any copyright notation herein. Additional funding was provided by the Materials for Extreme Dynamic Environments program sponsored by the US Army Research Laboratory Cooperative Agreement (W911NF-12-2-0022). Zeynep Aygüzer Yaşar acknowledges the graduate scholarship from the Ministry of National Education of the Republic of Turkey.

CONFLICT OF INTEREST

The authors declare that they have no conflicts of interest.

REFERENCES

1. Feinle, P. and Knoch, H., Product development with SiC and B₄C ceramics, *Proc. 3rd European Symp. on Engineering Ceramics*, Dordrecht: Springer, 1991.
2. Sahani, P., Karak, S.K., Mishra, B., Chakravarty, D., and Chaira, D., A comparative study on SiC–B₄C–Si cermet prepared by pressureless sintering and spark plasma sintering methods, *Metall. Mater. Trans. A*, 2016, vol. 47, pp. 3065–3076.
<https://doi.org/10.1007/s11661-016-3401-2>
3. Clark, H.K. and Hoard, J.L., The crystal structure of boron carbide, *J. Am. Chem. Soc.*, 1943, vol. 65, pp. 2115–2119.
<https://doi.org/10.1021/ja01251a026>
4. Lee, H. and Speyer, R.F., Pressureless sintering of boron carbide, *J. Am. Ceram. Soc.*, 2003, vol. 86, pp. 1468–1473.
5. Schmalzried, C. and Schwetz, K.A., Silicon carbide- and boron carbide-based hard materials, in *Ceramics Science and Technology*, vol. 2: *Materials and Properties*, Chichester: Wiley, 2010, Ch. 4, pp. 131–227.
6. Cho, N., Processing of boron carbide, *PhD Thesis*, Atlanta, GA: Sch. Mater. Sci. Eng., Georgia Inst. Technol., 2005.
7. Zhang, M., Zhang, W., Zhang, Y., and Gao, L., Fabrication, microstructure and mechanical behavior of SiCw–B₄C–Si composite, *Mater. Sci. Eng., A*, 2012, vol. 552, pp. 410–414.
<https://doi.org/10.1016/j.msea.2012.05.062>
8. Wang, Y.J., Peng, H.X., Ye, F., and Zhou, Y., Effect of TiB₂ content on microstructure and mechanical properties of in-situ fabricated TiB₂/B₄C composites, *Trans. Nonferrous Met. Soc. China*, 2011, vol. 21, pp. 1–5.
[https://doi.org/10.1016/S1003-6326\(11\)61608-7](https://doi.org/10.1016/S1003-6326(11)61608-7)
9. Zhang, Z., Du, X., Wang, W., Fu, Z., and Wang, H., Preparation of B₄C–SiC composite ceramics through hot pressing assisted by mechanical alloying, *Int. J. Refract. Met. Hard Mater.*, 2013, vol. 41, pp. 270–275.
<https://doi.org/10.1016/j.ijrmhm.2013.04.012>
10. Hayun, S., Paris, V., Dariel, M.P., Frage, N., and Zaretsky, E., Static and dynamic mechanical properties of boron carbide processed by spark plasma sintering, *J. Eur. Ceram. Soc.*, 2009, vol. 29, pp. 3395–3400.
<https://doi.org/10.1016/j.jeurceramsoc.2009.07.007>
11. Vargas-Gonzalez, L., Speyer, R.F., and Campbell, J., Flexural strength, fracture toughness, and hardness of silicon carbide and boron carbide armor ceramics, *Int. J. Appl. Ceram. Technol.*, 2010, vol. 7, pp. 643–651.
12. Narushima, T., Goto, T., Maruyama, M., Arashi, H., and Iguchi, Y., Oxidation of boron carbide-silicon carbide composite at 1073 to 1773 K, *Mater. Trans.*, 2003, vol. 44, pp. 401–406.
13. Groth, B.P., *On the Use of Raman Spectroscopy and Instrumented*, New Brunswick, NJ: Rutgers the State Univ., 2013.
14. Slusark, D.M., The effect of microstructural variation on the mechanical and acoustic properties of silicon carbide, *PhD Thesis*, New Brunswick, NJ: Rutgers the State Univ., 2012.
15. Lanfant, B., Leconte, Y., Bonnefont, G., Garnier, V., Jorand, Y., Le Gallet, S., Pinault, M., Herlin-Boime, N., Bernard, F., and Fantozzi, G., Effects of carbon and oxygen on the spark plasma sintering additive-free densification and on the mechanical properties of nanostructured SiC ceramics, *J. Eur. Ceram. Soc.*, 2015, vol. 35, pp. 3369–3379.
<https://doi.org/10.1016/j.jeurceramsoc.2015.05.014>
16. Schwetz, K.A., Silicon carbide based hard materials, in *Handbook of Ceramic Hard Materials*, Chichester: Wiley, 2000, Ch. 5.
17. Sadow, S.E. and Agarwal, A., *Advances in Silicon Carbide Processing and Applications*, Boston, MA: Artech House, 2004.
18. Saxena, K.K., Agarwal, S., and Khare, S.K., Surface characterization, material removal mechanism and material migration study of micro EDM process on conductive SiC, *Procedia CIRP*, 2016, vol. 42, pp. 179–184.
19. Izhevskiy, V., Genova, L., Bressiani, J., and Bressiani, A., Silicon carbide: Structure, properties and processing, *Ceramica*, 2000, vol. 46, pp. 4–13.
20. Paris, V., Frage, N., Dariel, M.P., and Zaretsky, E., The spall strength of silicon carbide and boron carbide ceramics processed by spark plasma sintering, *Int. J. Impact Eng.*, 2010, vol. 37, pp. 1092–1099.
<https://doi.org/10.1016/j.ijimpeng.2010.06.008>
21. Ogawa, I., Nishikubo, K., and Imamura, T., Growth of graphite particles in carbons/SiC/B₄C composites, *Carbon*, 1999, vol. 37, pp. 1000–1002.
22. Raju, K. and Yoon, D.-H., Sintering additives for SiC based on the reactivity: A review, *Ceram. Int.*, 2016, vol. 42, pp. 17947–17962.
<https://doi.org/10.1016/j.ceramint.2016.09.022>
23. Liang, H., Yao, X., Huang, Z., Zeng, Y., and Su, B., Effect of sintering techniques on the microstructure of liquid-phase-sintered SiC ceramics, *J. Eur. Ceram. Soc.*, 2016, vol. 36, pp. 1863–1871.
<https://doi.org/10.1016/j.jeurceramsoc.2016.01.018>

24. Šajgalík, P., Sedláček, J., Lenčič, Z., Dusza, J., and Lin, H.-T., Additive-free hot-pressed silicon carbide ceramics—A material with exceptional mechanical properties, *J. Eur. Ceram. Soc.*, 2016, vol. 36, pp. 1333–1341. <https://doi.org/https://doi.org/10.1016/j.jeurceramsoc.2015.12.013>
25. Du, X., Zhang, Z., Wang, W., Wang, H., and Fu, Z., Microstructure and properties of B₄C–SiC composites prepared by polycarbosilane-coating/B₄C powder route, *J. Eur. Ceram. Soc.*, 2014, vol. 34, pp. 1123–1129. <https://doi.org/10.1016/j.jeurceramsoc.2013.10.039>
26. Zhu, Y., Wang, F., Wang, Y., Cheng, H., Luo, D., and Zhao, Y., Mechanical properties and microstructure evolution of pressureless-sintered B₄C–SiC ceramic composite with CeO₂ additive, *Ceram. Int.*, 2019, vol. 45, pp. 15108–15115. <https://doi.org/10.1016/j.ceramint.2019.04.251>
27. Yaşar, Z.A. and Haber, R.A., Evaluating the role of uniformity on the properties of B₄C–SiC composites, *Ceram. Int.*, 2020, vol. 47, pp. 4838–4844. <https://doi.org/10.1016/j.ceramint.2020.10.055>
28. Moshtaghion, B.M., García, D.G., and Domínguez-Rodríguez, A., High-temperature plastic deformation of spark plasma sintered boron carbide-based composites: The case study of B₄C–SiC with/without graphite (g), *J. Eur. Ceram. Soc.*, 2016, vol. 36, pp. 1127–1134. <https://doi.org/10.1016/j.jeurceramsoc.2015.12.016>
29. Ivzhenko, V.V., Kaidash, O.N., Sarnavskaya, G.F., Dub, S.N., Popov, V.A., Bologova, L.M., and Lisovenko, S.A., Special features of the formation of the structure and properties of materials from the B₄C–TiH₂ powder system in reaction sintering under pressure, *J. Superhard Mater.*, 2011, vol. 33, pp. 34–43. <https://doi.org/10.3103/S1063457611010059>
30. Lankau, V., Martin, H.P., Hempel-Weber, R., Oeschler, N., and Michaelis, A., Preparation and thermoelectric characterization of SiC–B₄C composites, *J. Electron. Mater.*, 2010, vol. 39, pp. 1809–1813. <https://doi.org/10.1007/s11664-010-1129-0>
31. Sahani, P., Karak, S.K., Mishra, B., Chakravarty, D., and Chaira, D., Effect of Al addition on SiC–B₄C cermet prepared by pressureless sintering and spark plasma sintering methods, *Int. J. Refract. Met. Hard Mater.*, 2016, vol. 57, pp. 31–41. <https://doi.org/10.1016/j.ijrmhm.2016.02.005>
32. Uehara, M., Shiraiishi, R., Nogami, A., Enomoto, N., and Hojo, J., SiC–B₄C composites for synergistic enhancement of thermoelectric property, *J. Eur. Ceram. Soc.*, 2004, vol. 24, pp. 409–412. [https://doi.org/10.1016/S0955-2219\(03\)00213-9](https://doi.org/10.1016/S0955-2219(03)00213-9)
33. Bagiński, S.E., Effect of sintering time and composition of sintering aids on the core-rim microstructure and material properties of spark plasma sintered silicon carbide, *MSc Thesis*, New Brunswick, NJ, 2013.
34. Hulbert, D.M., Jiang, D., Dudina, D.V., and Mukherjee, A.K., The synthesis and consolidation of hard materials by spark plasma sintering, *Int. J. Refract. Met. Hard Mater.*, 2009, vol. 27, pp. 367–375.
35. *ASTM E494-10: Standard Practice for Measuring Ultrasonic Velocity in Materials*, West Conshohocken, PA: ASTM Int., 2010.
36. *ASTM C1327-15(2019): Standard Test Method for Vickers Indentation Hardness of Advanced Ceramics*, West Conshohocken, PA: ASTM Int., 2019.
37. Quinn, G.D., Salem, J., Bar-On, I., Cho, K., Foley, M., and Fang, H., Fracture toughness of advanced ceramics at room temperature, *J. Res. Natl. Inst. Stand. Technol.*, 1992, vol. 97, p. 579.
38. Zhang, W., Yamashita, S., and Kita, H., Effect of counterbody on tribological properties of B₄C–SiC composite ceramics, *Wear*, 2020, vols. 458–459, 203418. <https://doi.org/10.1016/j.wear.2020.203418>
39. Zhang, Z., Du, X., Li, Z., Wang, W., Zhang, J., and Fu, Z., Microstructures and mechanical properties of B₄C–SiC intergranular/intragranular nanocomposite ceramics fabricated from B₄C, Si, and graphite powders, *J. Eur. Ceram. Soc.*, 2014, vol. 34, pp. 2153–2161. <https://doi.org/10.1016/j.jeurceramsoc.2014.02.032>
40. Thuault, A., Marinell, S., Savary, E., Heuguet, R., Saunier, S., Goeriot, D., and Agrawal, D., Processing of reaction-bonded B₄C–SiC composites in a single-mode microwave cavity, *Ceram. Int.*, 2013, vol. 39, pp. 1215–1219. <https://doi.org/10.1016/j.ceramint.2012.07.047>
41. Hayun, S., Dilman, H., Dariel, M.P., Frage, N., and Dub, S., The effect of carbon source on the microstructure and the mechanical properties of reaction bonded boron carbide, in *Advances in Sintering Science and Technology: Ceramic Transactions*, Columbus, OH: Am. Ceram. Soc., 2010, pp. 27–39.
42. Dub, S.N., Kushch, V.I., Kaidash, O.N., Sereda, V.P., and Panasyuk, T.S., Initiation of a plastic flow in boron carbide at nanoindentation, *J. Superhard Mater.*, 2015, vol. 37, pp. 8–13. <https://doi.org/10.3103/S1063457615010025>
43. Zhang, Z., Du, X., Wang, W., Fu, Z., and Wang, H., Preparation of B₄C–SiC composite ceramics through hot pressing assisted by mechanical alloying, *Int. J. Refract. Met. Hard Mater.*, 2013, vol. 41, pp. 270–275. <https://doi.org/10.1016/j.ijrmhm.2013.04.012>